A Diagnostic Study of Moist Potential Vorticity Generation in an Extratropical Cyclone①

Zuohao Cao and *G.W.K. Moore*

Department of Physics, University of Toronto, Toronto, Ontario, Canada, M5S 1A7

Received September 12, 1997

ABSTRACT

Moist potential vorticity (MPV) and its generation may be important in the development of mesoscale structures such as rainbands within cyclones. In an adiabatic and frictionless flow, MPV generation is possible if the flow is three-dimensional *and* the air is unsaturated. Moist potential vorticity can be generated through the combined effects of gradients in the potential temperature and moisture fields. The diagnosis of MPV generation in an extratropical cyclone was performed with the ECMWF objectively analyzed fields for a system that developed during February 1992. It was found that at various stages during the development of the cyclone, negative MPV was generated: at the north end of the cold front; along the occluded front and the cold front; and in the region of the warm core. This pattern of negative MPV generation is in excellent agreement with the predictions of previous theoretical and numerical studies. After the cyclone ceased to deepen, the region of negative MPV generated in the cyclone was horizontally advected into a saturated area. The area of negative MPV generated both along the occluded front in this case study and in the region of the bent-back warm front in a numerical simulation showed a mesoscale structure with a width of about 200–500 km. It was found that the intrusion of moist or dry air into baroclinic zones was important for MPV generation. In addition, baroclinicity increase (adjacent to the area of condensation) in the regions of high moisture gradients led to significant MPV production.

Key words: Moist potential vorticity (MPV) generation, Extratropical cyclones

I. INTRODUCTION

Most precipitation in extratropical cyclones is organized at the meso-β scale (20–200 km) in the form of quasi two-dimensional structures known as rainbands. According to Houze et al. (1976), Hobbs (1978) and Matejka et al. (1980), the principal rainbands in extratropical cyclones can be classified into six types, i.e., warm-frontal, warm-sector, wide cold-frontal, narrow cold-frontal, postfrontal cold-surge, and postfrontal rainbands. Both theoretical studies (Bennetts and Hoskins, 1979; Emanuel, 1979) and observational studies (Parsons and Hobbs, 1983; Bennetts and Ryder, 1984) have suggested that conditional symmetric instability (CSI) may be a mechanism responsible for the organization of these rainbands.

Since CSI was first proposed as a mechanism for the formation of frontal rainbands, the concept of moist potential vorticity (MPV) has been extensively used in studies of CSI. Moist potential vorticity is defined as:

①Corresponding author: Dr. Zuohao Cao, Climate Processes and Earth Observation Atmospheric Environment Service, 4905 Dufferin Street, Downsview, Ontario, Canada M3H 5T4. E-mail: zuohao.cao@ec.gc.ca.

$$\frac{1}{\rho}\vec{\zeta}_a \cdot \nabla\theta_e, \tag{1}$$

where $\vec{\zeta}_a$, θ_e and ρ are the absolute vorticity vector equivalent potential temperature, and density respectively. It was shown by Bennetts and Hoskins (1979) that negative MPV is a sufficient condition for two-dimensional frictionless flow to be unstable to CSI. This condition was satisfied in several observed cases of extratropical cyclones (Bennetts and Sharp, 1982). Based on a fine-mesh model simulation of an observed case, Shutts (1990) showed that a substantial amount of available potential energy for CSI was present prior to explosive cyclone development. Furthermore, Reuter and Yau (1990) suggested that slantwise convection due to CSI is likely to be ubiquitous in extratropical cyclones. The negative MPV generation in extratropical cyclones is therefore crucial for understanding the role that CSI plays in the development of extratropical cyclones and their embedded mesoscale structures.

Despite the potentially important role played by MPV in the meso-scale structure of extratropical cyclones, there has been little work on elucidating the processes by which regions of negative MPV develop. In an adiabatic and frictionless flow MPV is materially conserved if the flow is two-dimensional, or if the flow is three-dimensional *and* the air is saturated. Moist potential vorticity generation is therefore possible if the flow is three-dimensional *and* the air is unsaturated (e.g., Bennetts and Hoskins, 1979). Based on a scaling analysis, Bennetts and Hoskins, (1979) suggested that the term defined as the dot product of the three-dimensional gradient of equivalent potential temperature and solenoidal term, which they referred to as the "solenoidal" term, could be an important term in the MPV budget equation. Recently, Persson (1995) quantified the importance of this term in a simulation of an observed case of a cold front. The MPV structure that developed in the Meteo-France mesoscale PERIDOT model was similar to that observed. The classification of this term is somewhat problematic. This term can be expressed as the *dot product* of the equivalent potential temperature *and* the solenoidal term in the absolute vorticity equation. In addition, this term involves both dry and moist processes which makes it difficult to clarify the relative importance of these processes in the generation of MPV. Cao and Cho (1995) performed a detailed derivation to clarify the physical processes responsible for the generation of MPV. They found that negative (positive) MPV can be generated in regions where the baroclinic vector, defined as the cross product of the three-dimensional gradients of potential temperature and pressure, has a component along (against) the direction of the moisture gradient. For these reasons, we choose not to use the nomenclature of Bennetts and Hoskins (1979) but will refer to the above term as the baroclinic-moisture term. Cao and Cho (1995) also performed numerical simulations using the PSU / NCAR three-dimensional hydrostatic mesoscale model (Anthes et al., 1987; Anthes, 1990) to verify this mechanism of MPV generation. They showed that at the different stages of cyclone development, negative MPV usually appears in the warm sector near the north part of the cold frontal zone, along the bent-back warm front and the cold front, and in the region of the warm core.

In this study, the diagnosis of MPV generation in an extratropical cyclone is carried out using objectively analyzed fields from the European Centre for Medium Range Weather Forecasting (ECMWF) to corroborate the results of Cao and Cho (1995). The system that was chosen to be analyzed occurred during a field project, the second phase of the Canadian Atlantic Storms Project (CASP II), whose aim was to investigate the processes responsible for

the generation of cyclones off the East Coast of Canada (Stewart, 1991). The time period for this study is from 0000 GMT February 8 to 1200 GMT February 11 1992, and includes the CASP II Intensive Observational Period (IOP) number 3.8.

II. OBJECTIVELY ANALYZED FIELDS

The ECMWF level III-A advanced surface and upper-air objectively analyzed fields (ECMWF 1992) obtained from the Data Support Section at NCAR were used in this study. Standard surface and upper-level fields are included in the analysis together with the other supplementary fields such as surface sensible and latent heat fluxes. The data assimilation model was run at a triangular truncation of T213 with 31 levels in the vertical. The III-A dataset is of a triangular truncation of T106 with 15 constant pressure levels at p = 1000, 925, 850, 700, 500, 400, 300, 250, 200, 150, 100, 70, 50, 30, and 10 hPa, respectively. The data are stored on a 320 × 160 grid and have been interpolated from the Gaussian grid to one with an equally spaced horizontal resolution of 1.125 degrees. The data are properly used with the full T106 resolution without truncation (Trenberth and Solomon, 1993). The fields are available 4 times daily (0, 6, 12, and 18 GMT).

To evaluate the accuracy of the ECMWF analyses, we compare the ECMWF analyses with observations in the region of interest. In the data sparse region where the cyclone event occurred, only a few stations are available for this comparison. Figures 1 and 2 show time-pressure cross-sections of specific humidity, temperature, zonal and meridional

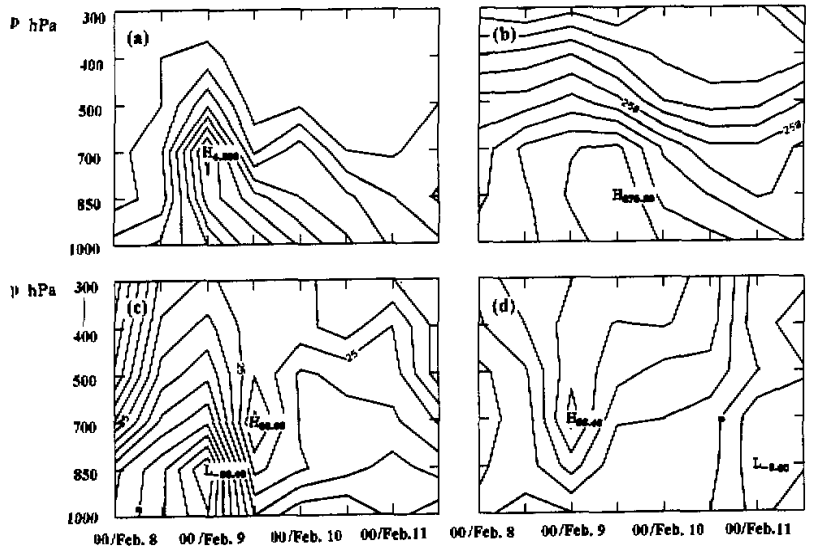

Fig.1. Time-pressure cross sections of observations made at St. John's, Newfoundland of (a) specific humidity at an interval of 0.5 g kg^{-1}, (b) temperature at an interval of 5 K, (c) zonal component of velocity at an interval of 5 ms^{-1}, and (d) meridional component of velocity at an interval of 5 ms^{-1}.

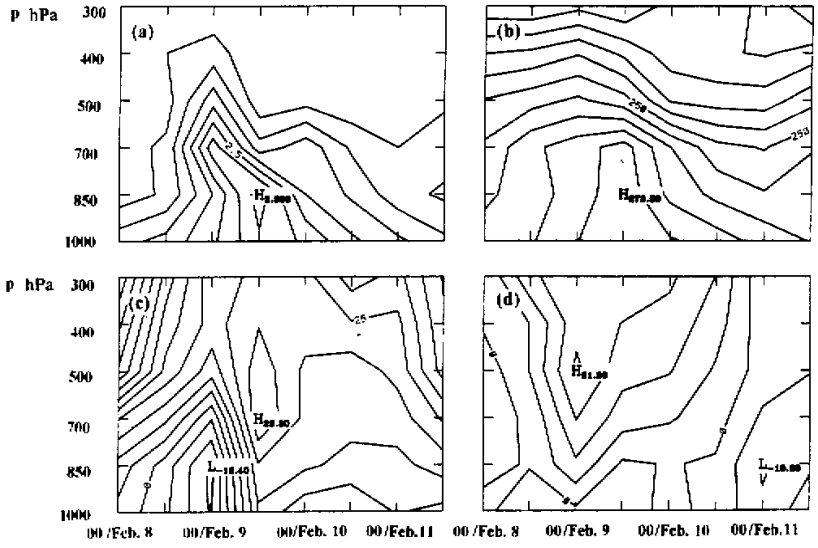

Fig.2. Same as Fig.1 except fields retrieved from ECMWF analyzed fields.

component velocities at St. John's, Newfoundland based on upper-air observations and ECMWF analyses, respectively. The moisture field is one of the most difficult fields to represent accurately in analyses (Trenberth and Solomon, 1993; Trenberth and Olson, 1988), but it is a very important field for this diagnostic study. As can be seen from Figs.1 and 2, the analyzed moisture field is in good agreement with the observed one in terms of distribution and magnitude. The other fields are also well verified against the observations (Figs.1b–d and 2b–d). We also compared the upper-air observations at Sable Island with the ECMWF analysis and found similar good agreement. Lacking observations over the ocean, it is reasonable to conclude, for this case at least, that the ECMWF's analysis is representative of the actual state of the atmosphere below the 300 hPa pressure surface.

III. DIAGNOSIS OF MPV GENERATION IN AN EXTRATROPICAL CYCLONE

1. *A Brief Description of the Cyclone*

The initial synoptic environment in this case study (Fig.3) is fairly similar to that of the idealized simulation in Cao and Cho (1995) (see their Fig.1). Both of them have a finite amplitude disturbance in the pressure field situated in a strong baroclinic zone. Although not shown, the relative humidity fields associated with both cyclones are distributed in such a way that low-level high moisture content air is located on their southeast flanks. It will be seen that the features of MPV generation in this cyclone compare favorably with predictions made by Cao and Cho (1995).

During the 36 hour period from 0000 GMT February 8 to 1200 GMT February 9 1992, the cyclone moved northeastward at a speed of approximately 15 ms^{-1}. The surface cyclone deepened little over this 36 hour period (Figs.3a–b). This cyclone initially developed in a

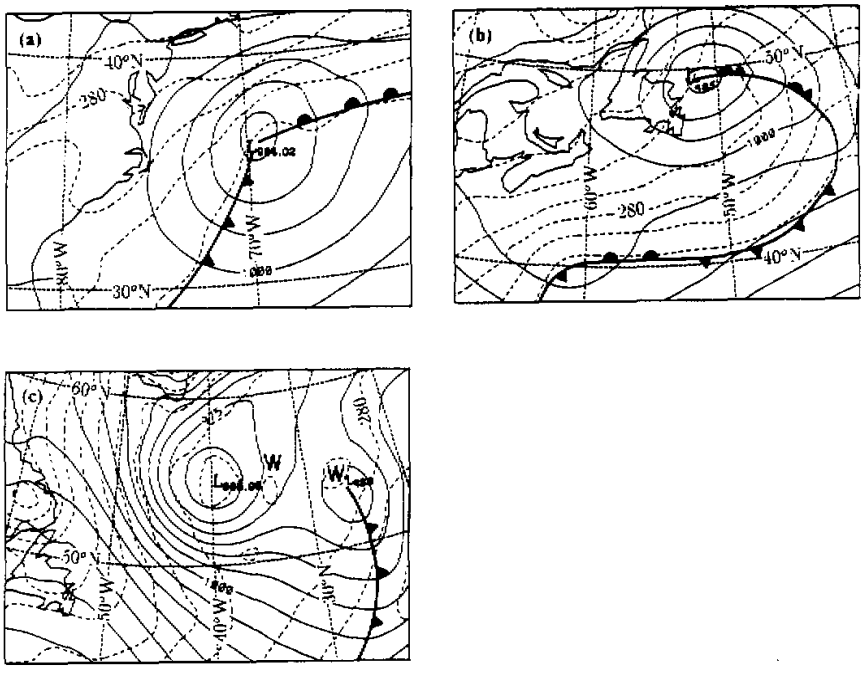

Fig.3. Sea-level pressure (solid lines) and temperature (dashed lines) fields at (a) 0000 GMT 8 February 1992, (b) 1200 GMT 9 February 1992, and (c) 1200 GMT 11 February 1992. The contour intervals of sea-level pressure and temperature are 5 hPa and 4 K, respectively. The fronts are superimposed onto the figures. "W" indicate the positions of warm cores.

strong baroclinic zone with the temperature gradient of about 28 K $(1500\ \text{km})^{-1}$ (Fig.3a). By 1200 GMT February 9 (Fig.3b), the cyclone approached Newfoundland meanwhile the occluded front formed.

Over the next two days from 1200 GMT February 9 to 1200 GMT February 11 the system moved slowly in a northeast direction at a speed of about 8.3 ms^{-1}. The cyclone deepened 20 hPa during this period. By 1200 GMT February 11, the cyclone was stationary and developed an interesting double-low structure (Fig.3c). The surface temperature field was similar to that at 0000 GMT February 11 (not shown), except that a stronger cold air advection behind the cold front was in favor of cyclone maintenance.

2. *Generation and Structure of MPV in the Cyclone*

Based on the theoretical analysis of Cao and Cho (1995), provided that the three-dimensional flow is frictionless and the air is unsaturated, the rate of change of MPV can be expressed as follows:

$$\frac{d}{dt}\left(\frac{\vec{\zeta}_a}{\rho} \cdot \nabla\theta_e\right) = A(\nabla\theta \times \nabla p) \cdot \nabla q, \tag{2}$$

where θ, p and q are potential temperature, pressure, and specific humidity fields,

respectively. The vector $\nabla\theta \times p$ is called the baroclinic vector and ∇q, is a three-dimensional moisture gradient. The quantity A is a function of θ,p and q and it has a negative value under typical atmospheric conditions (Cao and Cho, 1995). To qualitatively evaluate MPV generation on a constant pressure surface, the formula (2) can be re-written as

$$\frac{d}{dt}\left(\frac{\vec{\zeta}_a}{\rho} \cdot \nabla\theta_e\right) = A\left(\nabla_p\theta \times \frac{\partial p}{\partial n}\vec{n}\right) \cdot \nabla_p q, \tag{3}$$

where ∇p is a horizontal gradient operator on a constant pressure surface and $\vec{n}$ is the unit vector normal to the pressure surface. On a constant pressure surface, the baroclinic vector is parallel to the isolines of potential temperature. Its direction is 90° to the left of the potential temperature gradient. Hence, negative (positive) MPV will be generated in the regions where the angle between the baroclinic vector and the moisture gradient is less (larger) than 90°(Fig.4).

Figures 5 and 6 show the evolution of MPV and relative humidity fields on the 700 hPa pressure surface. As can be seen from Figs.5a and 6a, negative MPV was being generated at the north end of the cold front close to the surface low center, where the relative humidity varied from 30% to 60%. This pattern of negative MPV distribution in the cyclone is in excellent agreement with the simulated MPV at the early stage of cyclogenesis (Fig.5a of Cao and Cho (1995)). By 1200 GMT February 9, the negative MPV appeared in the region of the occluded front and behind the rear of the cold front. The magnitude of negative MPV in the vicinity of the occluded front was larger than that behind the cold front. By 1200 GMT February 11, with the appearance of the double-low structure and the enhancement of cold air advection to the west and southwest of the low center, the negative MPV in the region of 45°W to 52°W and 50°N to 60°N overlapped the condensation bands. At the same time, the negative MPV appeared in the regions of the warm cores (marked by W), and the negative values of MPV intensified along the cold front. It is interesting to note that there was a "dipole" structure of negative and positive MPV associated with the cold front, the occluded front, and the warm core (Figs.5a-c).

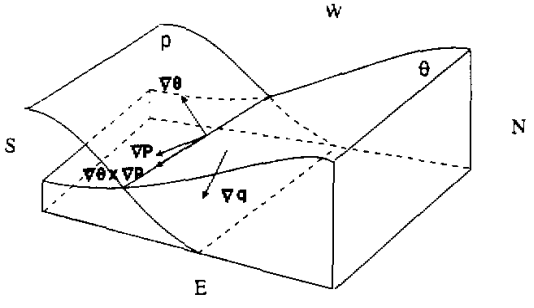

Fig.4. Schematic diagram of a baroclinic vector and moisture gradient in a frontal zone. $\nabla\theta$, ∇p, and ∇q represent the gradients of potential temperature, pressure, and specific humidity. N, S, E, and W stand for the North, South, East, and West.

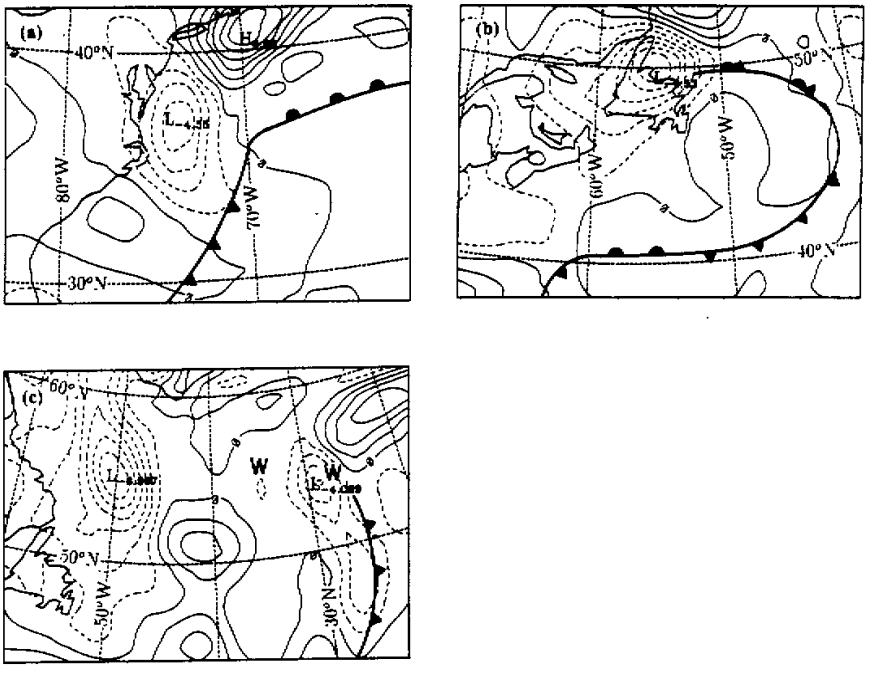

Fig.5. Moist potential vorticity on the 700 hPa pressure surface at (a) 0000 GMT 8 February 1992, (b) 1200 GMT 9 February 1992, and (c) 1200 GMT 11 February 1992. The contour interval is 1.0 $\times 10^{-7}$km^{2}kg^{-1}s^{-1} (=0.1 PVU). The dashed lines indicate the negative values of MPV. The fronts are superimposed onto the figures. 0W1s indicate the positions of warm cores.

Based on Eq.(3), the combined effects of baroclinicity and moisture gradients on MPV generation can be evaluated by plotting contours of potential temperature and specific humidity on a constant pressure surface. As a result, MPV is generated when thermal and moisture structures evolve relative to each other to produce intersecting gradients. For example, MPV is generated when a moist or dry air anomaly intrudes into a baroclinic zone, or when a thermal anomaly advects into a moisture zone. Fig. 7 shows potential temperature and specific humidity contours on the 700 hPa pressure surface at different stages of the cyclone evolution. At 0000 GMT February 8, tongues of moist air extended from the warm sector into the region close to the cyclone center, i.e., adjacent to the north end of the cold front and ahead of the warm front. A moisture core enclosed by 6 g kg^{-1} specific humidity contour was observed near the surface low center. This led to the significant changes of moisture gradients in the baroclinic zones and thereby MPV generation. Because the moisture gradients are antisymmetric around the moisture core, a dipole structure of MPV (Fig.5a) is generated in its vicinity (Fig.7a) provided that the thermal field does not have a warm or cold core in the same place and has at least some gradient. Another feature in Fig.7a was the intrusion of dry air behind the cold front into the baroclinic zones where it produced dramatic variations of moisture gradients along the cold frontal zones. This resulted in significant generation of negative MPV. Similarly, the thermal advection into the regions of high moisture gradients is also in favor of MPV generation.

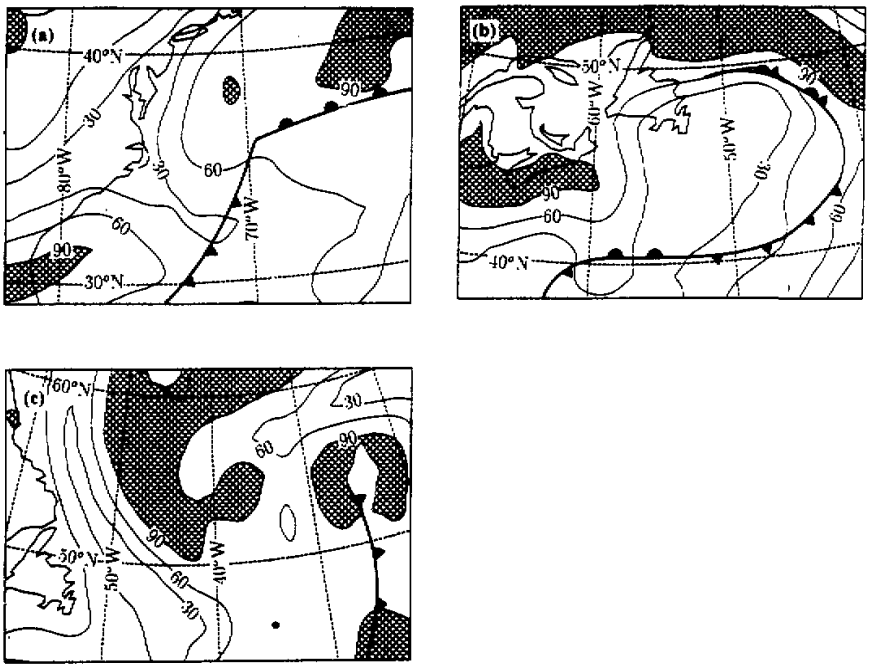

Fig.6. Relative humidity on the 700 hPa pressure surface at (a) 0000 GMT 8 February 1992, (b) 1200 GMT 9 February 1992, and (c) 1200 GMT 11 February 1992. The contour interval is 30% and the shadings indicate relative humidity larger than 90%. The fronts are superimposed onto the figures.

To gain further insight into the role of moisture and potential temperature distribution in MPV generation, we need to qualitatively examine the equations for the evolution of moisture and potential temperature gradients. In general, the evolution of moisture gradients on a constant pressure surface can be expressed as $\frac{d}{dt}|\nabla_p q|$, which is called a function M hereafter.

$$M = \frac{1}{|\nabla_p q|}\left[-\frac{\partial q}{\partial x}\left(\frac{\partial u}{\partial x}\frac{\partial q}{\partial x}+\frac{\partial v}{\partial x}\frac{\partial q}{\partial y}\right)-\frac{\partial q}{\partial y}\left(\frac{\partial u}{\partial y}\frac{\partial q}{\partial x}+\frac{\partial v}{\partial y}\frac{\partial q}{\partial y}\right)\right.$$
$$\left.-\frac{\partial q}{\partial x}\left(\frac{\partial w}{\partial x}\frac{\partial q}{\partial p}\right)-\frac{\partial q}{\partial y}\left(\frac{\partial w}{\partial y}\frac{\partial q}{\partial p}\right)+\frac{\partial q}{\partial x}\frac{\partial(e-c)}{\partial x}+\frac{\partial q}{\partial y}\frac{\partial(e-c)}{\partial y}\right], \quad (4)$$

where e is the rate of evaporation (plus sublimation) and c the rate of condensation (plus deposition) per unit mass. The first term represents the kinematic effect of confluence (diffluence) on the tendency of the horizontal moisture gradient. Confluence and diffluence contribute to both convergence and horizontal (nondivergent) deformation. Dry advection on the dry side and moist advection on the moist side increase the moisture gradient. The second term represents kinematically the tilting of the vertical moisture gradient onto the horizontal. Specific humidity usually decreases with height in the atmosphere. Rising motion on moist side and sinking motion on dry side increase the horizontal moisture gradient. The third term repre-

sents a horizontal variation in latent heating / cooling. For example, condensation on the moist side decreases the moist gradient while condensation on the less moist side increases the moisture gradient. Similarly, the evolution of potential temperature gradient, i.e., the frontogenetical function (Petterssen, 1936; Miller, 1948; Sanders, 1955; Bond and Fleagle, 1985; Raga et. al., 1994; Hanesiak et. al., 1997), can be expressed as

$$F=\frac{1}{\nabla_p\theta}\left[-\frac{\partial\theta}{\partial x}\left(\frac{\partial u}{\partial x}\frac{\partial\theta}{\partial x}+\frac{\partial v}{\partial x}\frac{\partial\theta}{\partial y}\right)-\frac{\partial\theta}{\partial y}\left(\frac{\partial u}{\partial y}\frac{\partial\theta}{\partial x}\right)+\frac{\partial v}{\partial y}\frac{\partial\theta}{\partial y}\right)-\frac{\partial\theta}{\partial x}\left(\frac{\partial w}{\partial x}\frac{\partial\theta}{\partial p}\right)-\frac{\partial\theta}{\partial y}\left(\frac{\partial w}{\partial y}\frac{\partial\theta}{\partial p}\right)+\frac{\pi}{C_p}\frac{\partial\theta}{\partial x}\frac{\partial\dot{Q}}{\partial x}+\frac{\pi}{C_p}\frac{\partial\theta}{\partial y}\frac{\partial\dot{Q}}{\partial y}\right], \tag{5}$$

where C_p, π, and $\dot{Q}$ are specific heat at constant pressure, the exner pressure, and diabatic heating, respectively. On the right hand side of Eq.(5), the first term stands for confluence (diffluence) effect on the tendency of the horizontal potential temperature gradient. Cold advection on the cold side and warm advection on the warm side increase the potential temperature gradient. The second term is the tilting of the vertical potential temperature gradient onto the horizontal. In a statically stable atmosphere, rising motion on the warm side and sinking motion on the cold side decrease the potential temperature gradient. The third term is horizontal variation of diabatic heating / cooling. For example, condensation on the warm side increases the potential temperature gradient while condensation on the cold side decreases the potential temperature gradient. The calculation of frontogenetical function F is highly resolution dependent. Bond and Fleagle (1985) compared the typical maximum values of frontogenetical terms such as confluence and tilting from several studies, and found that the maximum difference of those values is about 10^4–10^5 K m^{-1} s^{-1}. It seems that high resolution data are necessary for accurate calculations of the frontogenetical function. Similarly, it is expected to have high resolution data for accurate calculation of the function M. Raga et. al. (1994) performed the calculation of the frontogenetical function F with a resolution of 5 km in the horizontal and 100 m in the vertical. Hanesiak et. al. (1997) calculated the frontogenetical function F using the gridded data with a horizontal resolution of approximately 5 km and vertical resolution of 2 kPa. Both Raga et al. (1994) and Hanesiak et. al. (1997) show that confluence, tilting, and diabatic heating terms are of same order of magnitude. Because of relatively coarse resolutions of the data set used in this study (1.125 degree in horizontal and 15 layers from 1000 to 10 hPa in vertical), we did not attempt to calculate the terms in Eqs.(4) and (5). However, our purpose is to use those equations to qualitatively discuss where the moisture gradient zones can be expected to cross the baroclinic zones. It can be seen from Eqs.(4) and (5) that the different airstreams associated with the cyclone are important for the moisture gradient zones crossing the baroclinic zones. These airstreams usually include the warm conveyor belt ahead of the surface cold front, the cold conveyor belt originated from the easterly flow at low levels, and a dry airstream of subsided air behind the surface cold front (Carlson 1980; Browning, 1990). At the boundary between the dry airstream and the warm conveyor belt (Fig.9a), a strong confluence flow increased the moisture gradient due to the horizontally differentiated thermal advection. In addition, the downdraught behind the cold front in a dry air flow and the updraught in a warm moist conveyor belt made the vertical moisture gradient tilt onto the horizontal. Similarly, potential temperature gradients can be increased through these mechanisms. The calculation of the terms in Eqs. (4) and (5) gives the rate of change of moisture gradients and potential temperature gradients.

Due to the coarse resolution of the data set used in this study, we did not compute the individual terms in Eqs. (4) and (5) while we calculated the advection of specific humidity and potential temperature to see whether moisture advection or potential temperature advection is more important. Fig. 8 shows the three-dimensional advection of moisture and potential temperature at 0000 GMT February 8. To eliminate the effect of different units of moisture and potential temperature on the advection, the moisture advection and the potential temperature advection are divided by specific humidity and potential temperature, respectively. Comparisons between Fig. 8a and Fig. 8b indicate that the moisture advection is relatively more significant than the potential temperature advection. This explains why moisture gradient zones intrude into the potential temperature gradient zones.

When the cyclone arrived in Newfoundland at 1200 GMT February 9, condensation occurred (Fig.6b) in the neighborhood of the occluded front. Baroclinicity increased in the vicinity of condensation (refer to the third term of Eq.5), especially along the western part of the occluded front (Fig.7b). A warm core also developed to the south of the western part of the occluded front (Fig.7b). At this stage, the moisture gradients localized along the occluded frontal zone where the baroclinicity increased due to condensation, and negative MPV was therefore generated to the western part of the occluded front. By 1200 GMT February 11, the

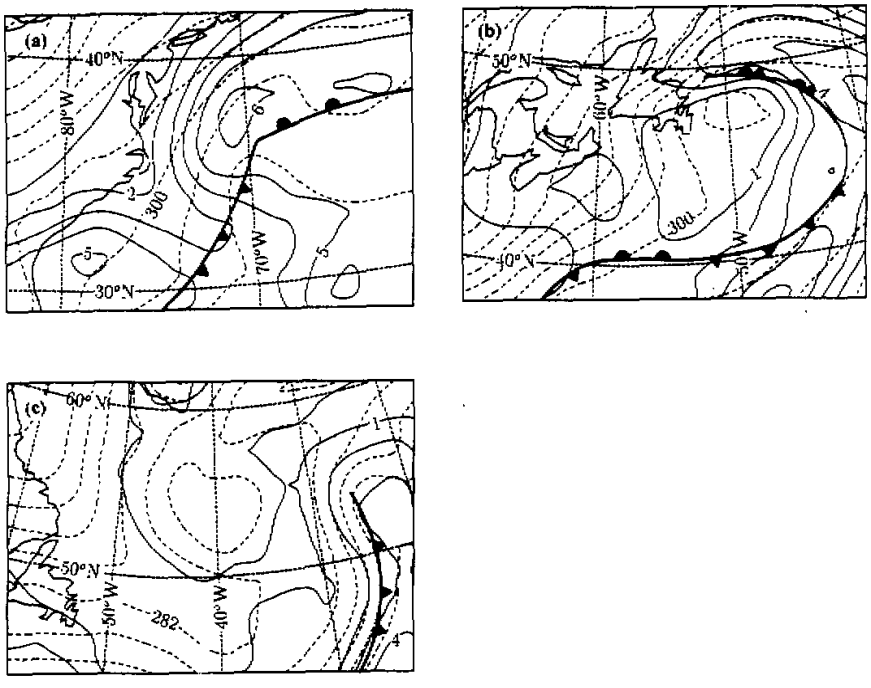

Fig.7. Distributions of specific humidity (solid lines) and potential temperature (dashed lines) on the 700 hPa pressure surface at (a) 0000 GMT 8 February 1992, (b) 1200 GMT 9 February 1992, and (c) 1200 GMT 11 February 1992. The contour intervals of specific humidity and potential temperature are 1 g kg^{-1} and 3 K, respectively. The analyzed fronts are superimposed onto the figures.

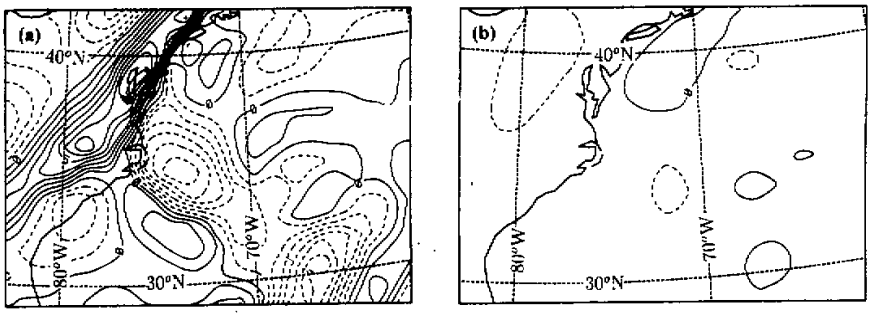

Fig.8. The horizontal distribution on the 700 hPa pressure surface at 0000 GMT 8 February 1992 of (a) $\vec{v} \cdot \nabla q / q$ at an interval of $1.0 \times 10^{5} s^{-1}$, and (b) $\vec{v} \cdot \nabla \theta / \theta$ at an interval of $1.0 \times 10^{-6} s^{-1}$.

negative MPV generation took place mainly along the cold front. Some of the negative MPV moved into a saturated environment (compare Fig.5c with Fig.6c), implying potential existence of CSI.

The MPV generation due to baroclinicity and moisture gradients can be understood from a different point of view by rewriting Eq.(3) in terms of the vertical derivative of geostrophic wind (proportional to the thermal wind). Under the assumption of the geostrophic wind balance Eq.(3) becomes

$$\frac{d}{dt}\left(\frac{\vec{\zeta}_a}{\rho} \cdot \nabla \theta_e\right) \mathbf{A} \rho T \left(\frac{\partial \vec{v}_g}{\partial n} \cdot \nabla_p q\right), \tag{6}$$

where T and $\vec{v}_g$ are temperature and geostrophic wind. Formula (6) is similar to the one given by Innocentini and Neto (1992) and Persson (1995) with the exception that we explicitly use specific humidity q rather than equivalent potential temperature θ_e. This makes the physical interpretation of the formula more clear. By comparing Eq.(3) with Eq.(6), one can see that the thermal wind is in the same direction as the baroclinic vector. Therefore, negative (positive) MPV can be generated in the region where the thermal wind has a component along (against) the moisture gradient. This physical explanation of MPV generation was first discussed by Bennetts and Hoskins (1979) in the Boussinesq framework. Since $\frac{\partial \vec{v}_g}{\partial n} \cdot \nabla_p q$ is a part of $\frac{\partial (\vec{v}_g \cdot \nabla_p q)}{\partial n}$, the baroclinic–moisture source term can be interpreted as the vertically differentiated moisture advection by the geostrophic wind (e.g., Persson, 1995). Negative MPV can be generated due to dry air advecting above moist air and reducing the moist static stability.

As described above, the analyses of the potential temperature and moisture fields on pressure surfaces give one a simple physical interpretation and qualitative information on MPV generation. A quantitative diagnosis of MPV generation can be completed by directly integrating Eq. (2):

$$MPV|_{t_2} - MPV|_{t_1} + \overline{\vec{v}_h \cdot \nabla_h (MPV)}\Delta t + \overline{w\frac{\partial (MPV)}{\partial p}}\Delta t = \overline{A(\nabla\theta \times \nabla p \cdot \nabla q)}\Delta t, \quad (7)$$

where the bar denotes the time average over the interval $\Delta t = t_2 - t_1$. As an example, we have chosen Δt to be the 6 hour period from 0600 GMT to 1200 GMT February 9. This equation represents the balance between the time-integrated total derivative of MPV and the time-integrated baroclinic-moisture term. During this period, negative MPV generation occurred mainly in the region of the western part of the occluded front near St. John's Newfoundland. To look at the detailed structure of MPV generation, we focus on this area. The region of interest is from 45°W to 70°W and from 39°N to 54°N. Fig. 9a shows the time-integrated baroclinic-moisture source term and Figs.9b–9d the time-integrated total derivative of MPV, the time-integrated horizontal and vertical advection of MPV. As can be seen from Figs.9a–9b, MPV generation is well balanced by the baroclinic-moisture source term, and the residual is small. In the occluded frontal region to the south of St. John's, the residual is about 9%. The maximum rate of MPV generation due to the baroclinic moisture process is about 9.2 PVU / day in the region of the western part of the occluded front. The horizontal MPV advection represents a major term in the MPV budget (Fig. 9c). It is two to three times larger than the vertical MPV advection (Fig. 9d). This quantitative diagnosis of MPV generation is quite representative of the results at other times even though we show the results only at this particular time.

3. *Other Factors That Affect the MPV Distribution*

In the previous section, we diagnosed one of the major sources of MPV generation that is governed by the baroclinicity and moisture gradients. This source term is referred to as the baroclinic-moisture term of MPV generation. In reality, however, the atmosphere is dissipative and diabatic, both of which affect the MPV distribution. The effect of a turbulent boundary layer (e.g., friction and fluxes of heat and momentum) is confined to 1–2 km above the Earth's surface, and has no direct influence on MPV generation in a free atmosphere (e.g., the 700 hPa pressure surface). However, MPV generation due to these turbulent boundary layer processes (initially located near the surface) can be transported upward. Moist potential vorticity generated from the baroclinic-moisture process may be mixed with MPV generated due to the boundary layer effects. The magnitude of vertical MPV advection is therefore very important in understanding whether the baroclinic-moisture or boundary layer processes are dominant in MPV generation. As shown in Figs.9c and 9d, the magnitude of vertical MPV advection is approximately one third that of horizontal MPV advection. The MPV advection is therefore dominated by horizontal transport at least for this case.

The effect of radiation on MPV generation in general is very small, except within a very thin layer, such as near the top of the cloud. Cao and Cho (1995) showed that the rate of MPV generation due to radiation is at least ten times smaller than that due to the baroclinic-moisture effect. In addition, as MPV generation induced by baroclinic-moisture effects takes place only in unsaturated regions, microphysical processes such as freezing and deposition (condensation has no effect on MPV generation) do not overlap the regions of MPV generated due to baroclinic-moisture effect. Rainwater evaporation usually occurs in substantially unsaturated downdraughts, but its effect on MPV generation is negligible because rainwater evaporation spreads over a deep column (Clough and Franks, 1991) and only generates a weak vertical gradient of diabatic cooling. This was also verified in the numerical

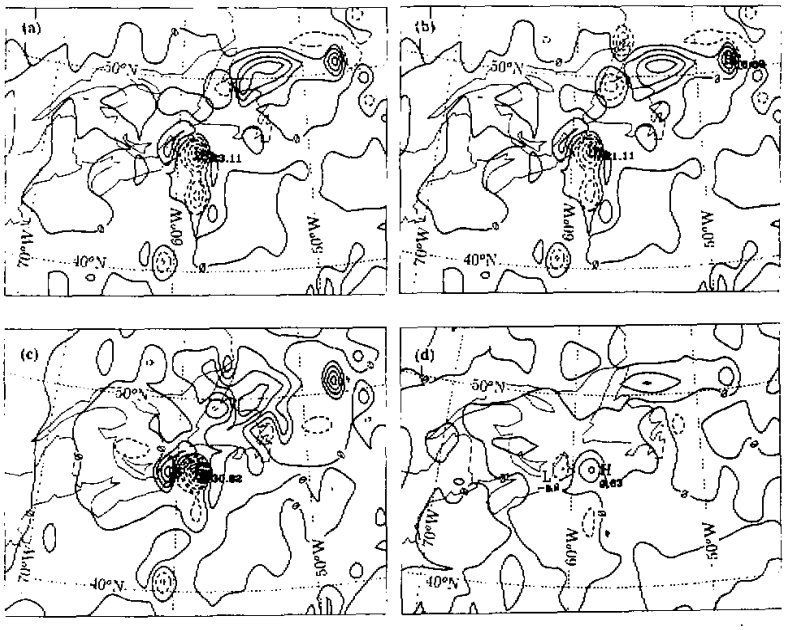

Fig.9. The horizontal distribution of (a) the time-integrated baroclinic moisture source term, (b) the time-integrated total derivative of MPV, (c) the time-integrated horizontal, and (d) vertical advection of MPV on the 700 hPa pressure surface. The integration is over 6 hour period from 0600 GMT to 1200 GMT 9 February 1992. The contour interval is 4.0×10^{-7} km^{2}kg^{-1}s^{-1} (=0.4 PVU).

simulation of Cao and Cho (1995). Processes of melting and sublimation frequently give rise to much stronger vertical gradients of diabatic cooling than rainwater evaporation. The effects of these processes are not examined in this paper although they might be also important for MPV generation in a localized region.

VI. DISCUSSION

Further comparisons can be made between this case study and the idealized numerical simulation of Cao and Cho (1995). The first point of comparison is the initial synoptic environment for cyclogenesis. As documented in Fig.3, the cyclones both in this case study and in the idealized numerical simulation initially developed in a very strong baroclinic zone. The initial surface temperature contrast (within 1500 km) was about 28 K in the case study, compared to 24 K in the idealized simulation. Initial finite pressure disturbances with closed isobars were observed in both cases. The detailed structural differences do not lead to differences of MPV generation patterns between the case study and the idealized simulation.

The pattern of MPV generation in the case study is in excellent agreement with that of the idealized simulation (Cao and Cho, 1995). It was found in the case study that negative

MPV generation at the different stages appeared at the north end of the cold front, along the occluded front and the cold front, and in the region of the warm core. At the mature stage, the negative MPV along the occluded front in the case study was about 1500 km in length and 500 km in width (Fig.5b); versus, in the idealized simulation, 1500 km in length and 200 km in width (Fig.5b of Cao and Cho, 1995).

This diagnostic study shows that the baroclinic-moisture generated MPV is important in the real atmosphere. The generated MPV in this cyclone event is mainly horizontally transported. In the idealized simulation, however, strong vertical transport of the generated MPV occurs. Once the negative MPV appears in saturated regions through horizontal and / or vertical transport, CSI may take place and thus slantwise convection may be initiated. A further discussion on the role of CSI in extratropical cyclones is beyond the scope of this paper simply because of the coarse resolution of the ECMWF analyzed fields.

V. CONCLUSIONS

Moist potential vorticity generation in an extratropical cyclone was diagnosed using ECMWF analyzed fields for the period from 0000 GMT February 8, 1992 to 1200 GMT February 11, 1992. Following the evolution of the cyclone, it was found that negative MPV was generated at the north end of the cold front, along the occluded front and the cold front, and in the region of the warm core. These patterns of negative MPV generation in this extratropical cyclone agree with the predictions of theoretical work and numerical simulations by Cao and Cho (1995). It was also found that the intrusion of moist or dry air into baroclinic zones, and baroclinicity increase (adjacent to the area of latent heat release) in the regions of high moisture gradients are two importantt processes for MPV generation.

After the negative MPV was generated, it was horizontally transported into a saturated region. In contrast to the MPV simulation in an idealized cyclone, the vertical transport of negative MPV was very small.

We would like to thank the Data Support Section of the National Center for Atmospheric Research for the ECMWF data. We express our appreciation to Robert Crawford for providing the CASP II data, and to Dr. Ian Renfrew for his comments in reading through the paper, and to P. King for discussion on frontal analyses. Funding for this research was provided by Atmospheric Environment Service through the Canadian Institute for Climate Research.

REFERENCES

Anthes, R.A., E.-Y. Hsie and Y.-H. Kuo (1987), Description of the Penn State / NCAR Mesoscale Model Version 4(MM4), NCAR Technical Note, NCAR / TN-282, 66pp.

Anthes, R. A. (1990), Recent applications of the Penn State / NCAR mesoscale model to synoptic, mesoscale, and climate studies, *Bull. Amer. Meteor. Soc.*, **71**: 1610-1629.

Bennetts, D. A. and B. J. Hoskins (1979), Conditional symmetric instability - a possible explanation for frontal rainbands, *Q. J. R. Met. Soc.*, **105**: 945-962.

Bennetts, D. A. and P. Ryder (1984), A study of mesoscale convective bands behind cold fronts, Part I: Mesoscale organization, *Q. J. R. Met. Soc.*, **110**: 121-145.

Bennetts, D. A. and J. C. Sharp (1982), The relevance of conditional symmetric instability to the precipitation of mesoscale frontal rainbands, *Q. J. R. Met. Soc.*, **108**: 595-602.

Bond, N. A. and R. G. Fleagle (1985), Structure of a cold front over the ocean, *Q. J. R. Met. Soc.*, **111**: 739-759.

Browning, K. A. (1990), Organization of clouds and precipitation in extratropical cyclones, Extratropical cyclones, The Erik Palmen Memorial Volume, C. W. Newton and E. Holopainen, *Eds. Amer. Meteor. Soc.*, **132**.

Cao, Z. and H.-R. Cho (1995), Generation of moist potential vorticity in extratropical cyclones, *J. Atmos. Sci.*, **52:** 3263-3281.

Carlson, T. N. (1980), Airflow through midlatitude cyclones and the comma cloud pattern, *Mon. Wea. Rev.*, **108:** 1498-1509.

Clough, S. A. and R. A. A. Franks (1991), The evaporation of frontal and other stratiform precipitation, *Q. J. R. Met. Soc.*, **117:** 1057-1080.

ECMWF (1992), The description of the ECMWF / WCRP Level III-A global atmospheric data archive, Available from the European Center for Medium Range Weather Forecasts.

Emanuel, K. A. (1979), Inertial instability and mesoscale convective systems, Part I: Linear theory of inertial instability in rotating viscous fluids, *J. Atmos. Sci.*, **36:** 2425-2449.

Hanesiak, J. M., R. E. Stewart, and K. K. Szeto et al. (1997), The structure, water budget and radiational features of a high latitude warm front, *J. Atmos. Sci.* (in press).

Hobbs, P. V. (1978), Organization and structure of clouds and precipitation on the mesoscale and microscale in cyclonic storms, *Rev. Geophys. Space Phys.*, **16:** 741-755.

Houze, R. A., P. V. Hobbs, K. R. Biswas and W. M. Davis (1976), Mesoscale rainbands in extratropical cyclones, *Mon. Wea. Rev.*, **104:** 868-878.

Innocentini, V. and E. D. S. C. Neto (1992), A numerical study of the role of humidity in the updraft driven by moist slantwise convection, *J. Atmos. Sci.*, **49:** 1092-1106.

Matejka, T. J., R. A. Houze and P. V. Hobbs (1980), Microphysics and dynamics of clouds associated with mesoscale rainbands in extratropical cyclones, *J. Roy. Meteor. Soc.*, **106:** 29-56.

Miller, J. E. (1948), On the concept of frontogenesis, *J. Meteor.*, **5:** 169-171.

Parsons, D. B. and P. V. Hobbs (1983), The mesoscale and microscale structure and organization of clouds and precipitation in mid-latitude cyclones. XI: Comparisons between observational and theoretical aspects of rainbands, *J. Atmos. Sci.*, **40:** 2377-2397.

Persson, P. O. G. (1995), Simulations of the potential vorticity structure and budget of Fronts 87 IOP8, *Q. J. R. Met. Soc.*, **121:** 1041-1081.

Petterssen, S. (1936), Contribution to the theory of frontogenesis, *Geophfys. Publ.*, **11**.

Raga, G. B., R. E. Stewart and J. W. Strapp (1994), Mesoscale structure of precipitation bands in a north Atlantic winter storm, *Mon. Wea. Rev.*, **122:** 2039-2051.

Reuter, G. W. and M. K. Yau (1990), Observations of slantwise convective instability in winter cyclones, *Mon. Wea. Rev.*, **118:** 447-458.

Sanders, F. (1955), An investigation of the structure and dynamics of an intense surface frontal zone, *J. Meteor.*, **12:** 542-552.

Shutts, G. J. (1990), Dynamical aspects of the October storm (1987), A study of a successful fine-mesh simulation, *Q. J. R. Met. Soc.*, **116:** 1315-1347.

Stewart, R. E. (1991), Canadian Atlantic Storms Program: Progress and plans of the meteorology component, *Bull. Amer. Meteor. Soc.*, **72:** 364-371.

Trenberth, K. E. and J. G. Olson (1988), An evaluation and intercomparison of global analyses from the National Meteorological Center and the European Center for Medium Range Weather Forecasts, *Bull. Amer. Meteor. Soc.*, **69:** 1047-1056.

Trenberth, K. E. and A. Solomon (1993), Implications of global atmospheric spatial spectra for processing and displaying data, *J. Climate*, **4:** 531-545.